CHAPTER 2

EXPERIMENTAL METHODS AND TECHNIQUES

This chapter gives necessary experimental procedures adopted for the synthesis of nanoparticles of Ag, Au, Cu and their alloys. The chemicals utilized for producing them are tabulated. Following a brief description of the synthesis protocol in the form of flow charts, working principles of various characterization tools are presented. Out of these, extensive utilization of transmission electron microscope (TEM) has been made in the thesis to investigate the structures, morphology, and chemistry of nanoparticles. The salient features of diffrerent imaging modes of TEM is presented. UV-Vis spectrophotometer was utilized to study LSPR behavior of the sols.

2.1 Materials and Methods

2.1.1 Chemical used

All the chemicals in the synthesis were of analytical reagent grade. They were used as received without further purification. Table 2.1 gives the details of the reagent used.

2.1.2 Synthesis Methods

The methods adopted to synthesize nanoparticles of Ag, Au, Cu, and their alloys in this doctoral thesis relate to two distinct categories. They refer to (a) green and (b) synthetic

TABLE 2.1: Name, chemical formula and manufacturer name of reagents used.

Sl. No.	**Chemical name**	**Chemical formula**	**Molecular wt. (g)**	**Company name**
1	Silver Nitrate	$AgNO_3$	169.87	Alfa Aesar
2	Chlroauric acid	$HAuCl_4.3H_2O$	393.82	Alfa Aesar
3	Cupric Nitrate	$Cu(NO_3)_2.3H_2O$	241.60	Merck
4	Cupric Chloride	$CuCl_2.2H_2O$	170.48	Merck
5	Glucose	$C_6H_{12}O_6$	180.16	Alfa Aesar
6	Hydrazine Hydrate	$N_2H_4.H_2O$	50.06	Merck
7	Sodium borohydride	$NaBH_4$	37.83	Merck
8	Poly-vinyl pyrrolidone (PVP)	$(C_6H_9NO)_n$	40,000	Himedia
9	Hexadecylamine (HDA)	$CH_3\ (CH_2)_{15}NH_2$	241.46	Alfa Aesar
10	Rice	-	-	Local grocery
11	Sodium hydroxide	NaOH	40	Merck
12	Oleylamine	$C_{18}H_{37}N$	267.49	Merck
13	Oleic acid	$C_{18}H_{32}O_2$	282.47	Merck
14	N,N-Dimethylformamide (DMF)	$HCON(CH_3)_2$	73.09	Merck

polymer based syntheses. They will be discussed in this chapter. The detail is given in experimental sections of respective chapters.

2.1.2.1 Synthesis of Ag, Au, and Cu Nanoparticles

The general synthesis protocol adopted is given schematically in Figure 2.1. Precursor solutions of Ag, Au, and Cu mentioned in table 2.1 were mixed thoroughly with rice-starch (rice gruel) solution. Rice-starch acted as reducing agent and stabilizer for formation of nanoparticles of Ag and Au. The hydrazine hydrate (HH) and rice-starch was used as reducing agent and stabilizer respectively to synthesize Cu nanoparticles (cf. chapter 3).

2.1.2.2 Synthesis of Ag-Cu and Au-Cu Alloy Nanoparticles

The synthesis of alloy nanoparticles of Ag-Cu and Au-Cu was carried out by two step method. At first, Cu NPs was prepared by method described in the previous section, followed by addition of Ag and Cu precursors in appropriate concentration. Rice-starch was used as stabilizing agent in these syntheses and process is shown in Figure 2.2 (cf. chapter 4). The solution phase syntheses employing other polymeric process is presented from here onwards.

2.1.2.3 Synthesis of facetted Au nanoparticles

Seed based synthesis was adopted to grow facetted Au NPs. The complete protocol is presented by a schematic and is shown in Figure 2.3. Chloroauric acid, NaBH4 and PVP served as precursor, reducing agent, and stabilizer, respectively, for seed crystals. A

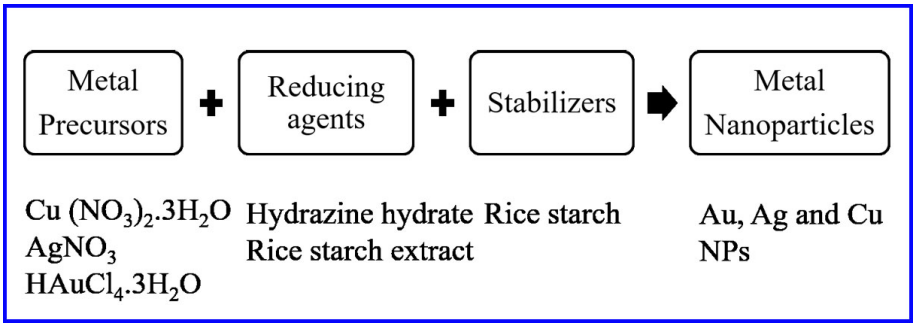

FIGURE 2.1: Scheme of synthesis protocol adopted for Ag, Au and Cu NPs.

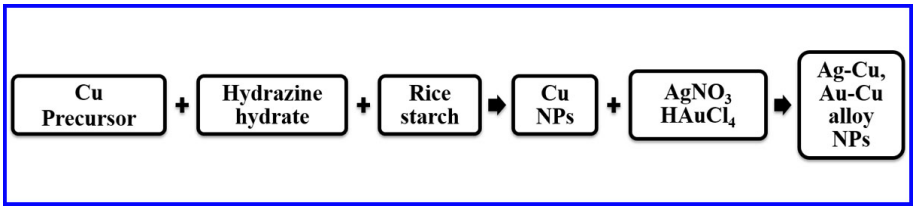

FIGURE 2.2: Schematic representation of synthesis method utilized for Ag-Cu and Au-Cu alloy NPs.

mixture of DMF and deionized water was used as solvent. Subsequently, seed was added in a growth solution containing Au precursor mixed with PVP in DMF solvent (cf. chapter 5).

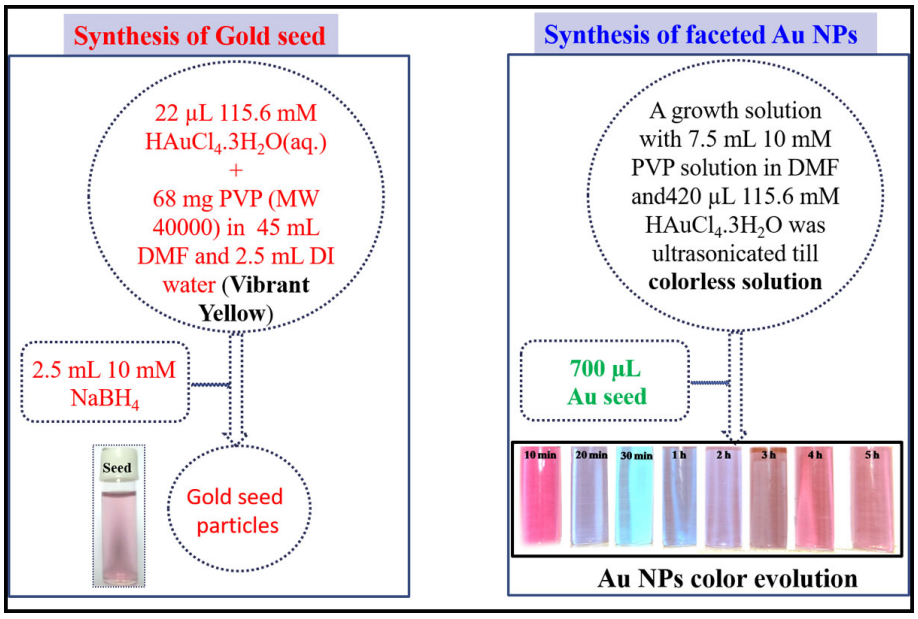

FIGURE 2.3: Illustration of synthesis steps used to synthesize faceted Au NPs.

2.1.2.4 Synthesis of Au-Cu nanostructures

The aqueous phase synthesis was achieved through reducing precursors of Au (chloroauric acid) and Cu (cupric chloride) simultaneously by glucose in presence of hexadecylamine as stabilizer. The temperature during synthesis was kept at 80 ^{o}C. The procedure adopted to prepare Au-Cu nanostructures is presented in Figure 2.4 (cf. chapter 6).

2.1.2.5 Synthesis of Au-Cu intermetallic nanoparticles

A single pot three step synthetic strategy was adopted to synthesize Au-Cu intermetallic nanoparticles. They refer to formation of Au seed in the first step and subsequent heat

treatments at temperatures 180 ^{o}C and 290 ^{o}C in solution phase. Here, a mixture of oleylamine and oleic acid was used as solvent, reducing agent, and stabilizer. The details are presented in Figure 2.5 with a schematic diagram (cf. chapter 7).

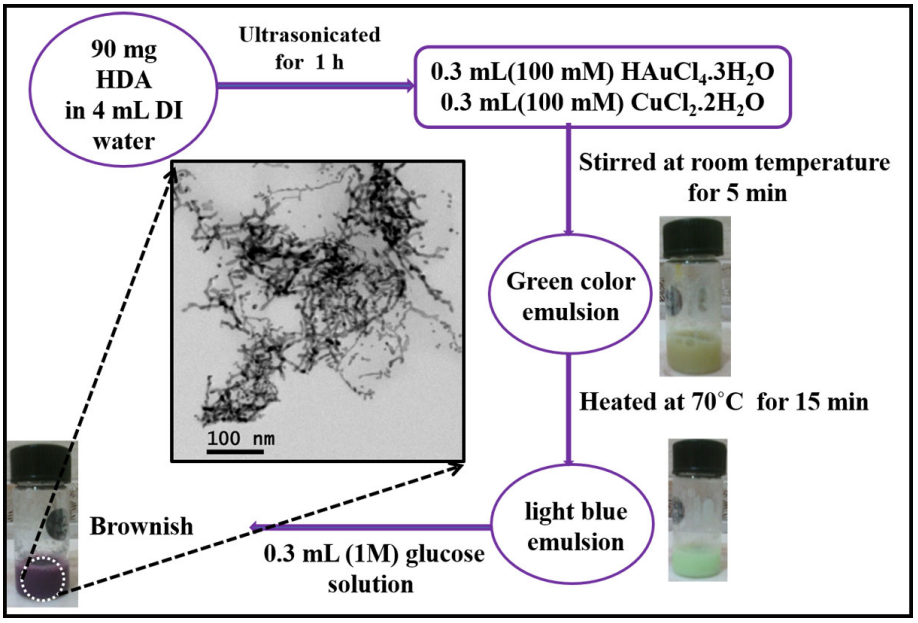

FIGURE 2.4: Schematic diagram showing reaction prorocol for synthesis of Au-Cu NPs.

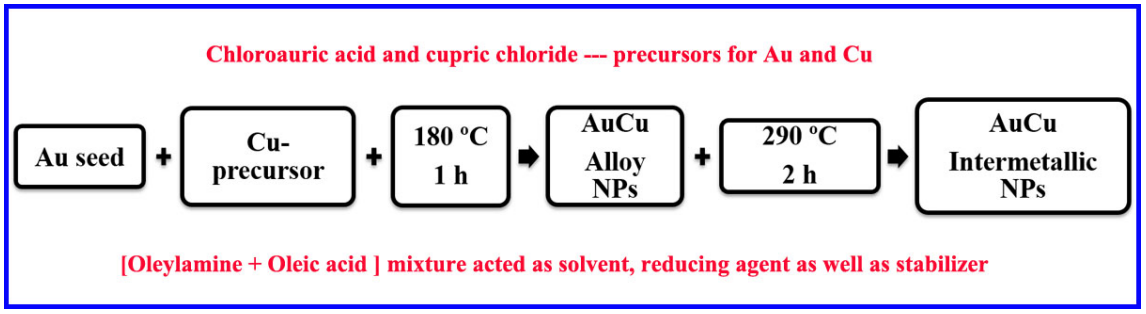

FIGURE 2.5: Schematic diagram showing single pot three step synthesis of Au-Cu intermetallic NPs.

2.2 Transmission Electron Microscope (TEM)

2.2.1 Principles of TEM

Light microscopes employs wavelength of visible light, thereby it has limitation of the image resolution ($\sim$ 200 nm). In contrast, electrons may display both wave and particle like behaviours as postulated by Louis de Broglie (1925). The wavelength is a function of accelerating voltage. Electrons could be focused onto a sample and could provide a resolution far better than that of the light microscopes. Electrons can have far shorter wavelength than that of light wave. One may realize that transmission electron microscope (TEM) operates on the same basic principles as the light microscope but uses electrons instead of light [141, 142]. TEM becomes the most efficient and tremendously powerful tool for the characterization of nanomaterials down to atomic levels. TEM can provide almost all the structural, phase, and crystallographic information of different materials because it can not only operate in real space to form images but also can provide information in reciprocal space in the form of diffraction pattern (DP). Generally, TEM includes several principal parts as follows: electron gun, electro-magnetic lens systems, vacuum chamber, viewing system [143]. There are two types of electron guns: one is the thermionic gun (producing electron when filament is heated) and the other is field-emission gun (producing electron when an intense electric field is applied to filament). The electron beam emitted from electron gun, gets diffracted when passing through thin crystalline specimen and form image or DP. Therefore, one needs to prepare specimen thin enough for electron transparency in TEM, which is quite a tedious process and a limitation of TEM.

2.2.2 TEM working/operating process

Figure 2.6 shows the profile and schematic ray diagram of the TEM [144]. The electrons are accelerated to 200kV in the LaB_6 thermal electron gun. The first condenser lens function is to create a demagnified image of the gun crossover and control the minimum spot size obtainable in the rest of the condenser system. Second condenser lens converges the beam at the specimen and control the diameter of the illuminated area of the specimen. The condenser aperture controls the fraction of the beam that hits the specimen and the intensity of illumination. This aperture increases resolution but degrades intensity and there is a tradeoff whenever an aperture is used. The objective lens forms an inverted initial image, which is subsequently magnified. Both the diffracted and unscattered electrons are focused by the objective lens. A diffraction pattern is formed at the back focal plane of the objective lens. The sample sits within the objective lens. The objective aperture is placed in the back focal plane of the image. Its function is to select those electrons, which will contribute to the image, and thereby affect the appearance of the image, improving the contrast of the final image. Below the objective aperture is the field limiting aperture or more commonly called as the selected area diffraction aperture. Its role is to allow the selection of an area of a sample to contribute to the diffraction pattern. The first intermediate lens can be focused on either the initial image formed by the objective lens, or the diffraction pattern formed at the back focal plane of it magnifies the image by a constant factor and determines whether the viewing screen shows a diffraction pattern or an image. Magnification in the electron microscope can be varied from hundreds to several hundred thousands times. This is done by varying the strength of the second intermediate lens and

the projector lens.

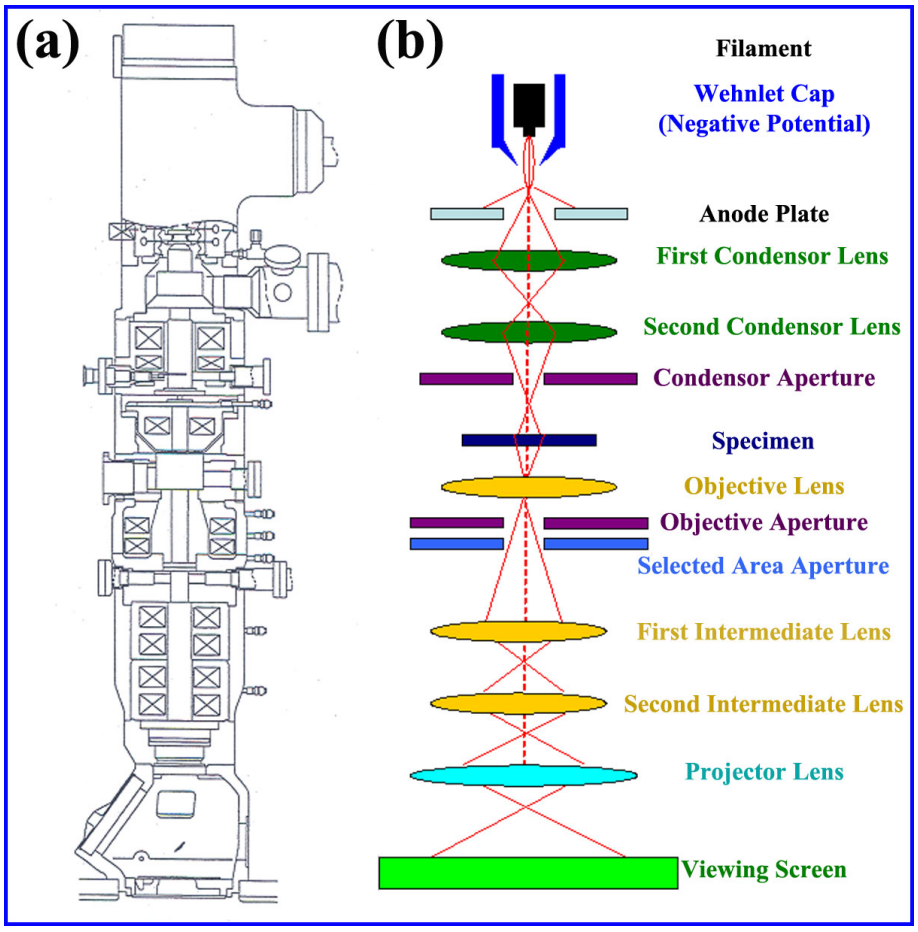

FIGURE 2.6: (a) Profile of TEM column section, (b) schematic ray diagram of TEM [144].

2.2.3 Electron diffraction pattern and image formation in TEM

As mentioned previously, there are two basic operations of TEM imaging system: one is the DP projection and the other is image projection. The diffraction method provides a way to study the crystal structures since informartion contained in DP could be used to reveal crystal structures [146]. When electron beam passes through the electron transparent area of the specimen, some electrons get scattered. After the electron beam passes

through objective lens, the DP will be formed at the back focal plane and image will be formed at image plane at the same time but at different positions [147, 148]. Figure 2.7 shows the ray diagram of the comparison of the formation of image and DP in the TEM. In order to get DP, one has to remove the objective aperture and insert the selected area diffraction (SAD) aperture at the same time, and then adjust the intermediate lens to select the DP formed at the back focal plane as the object plane for the intermediate lens, therefore, DP can be projected onto the viewing screen (Figure 2.7a). Instead, if one inserts the objective aperture and removes the SAD aperture, the image formation will take place at the image plane. One can adjust intermediate lens to select the image plane as the object plane of the intermediate lens, thus one may get the image onto a viewing screen (Figure 2.7 b) [145].

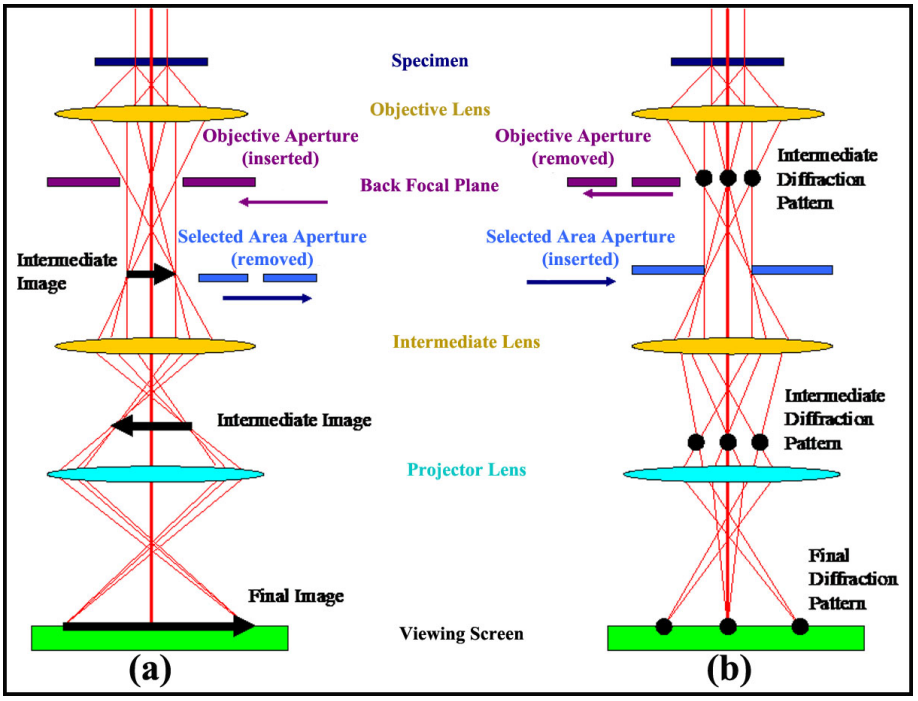

FIGURE 2.7: Ray diagram of (a) image and (b) DP formation in the TEM [145].

2.2.4 Bright filed and dark field images

There are two basic imaging operations in TEM, one is bright field (BF) image and the other is dark field (DF) image. When the electron beam passes through the specimen, there will be unscattered electrons which form central/direct beam and coherently scattered electrons will form diffracted beam. By inserting the objective aperture at the back focal plane of objective lens, one can choose the formation of bright field and dark field images separately [145], as the ray diagrams shown in Figure 2.8. Figure 2.8 schematically displays the ray diagrams of BF and DF image formation processes, respectively. If one works with direct beam (unscattered electrons) passing through the objective aperture (cf. Figure 2.8 a),then the resultant image formed on the viewing screen is called BF image. On the other hand, if one blocks the direct beam and allow the diffracted beam to pass through the objective aperture, the resultant image formed is called DF image as

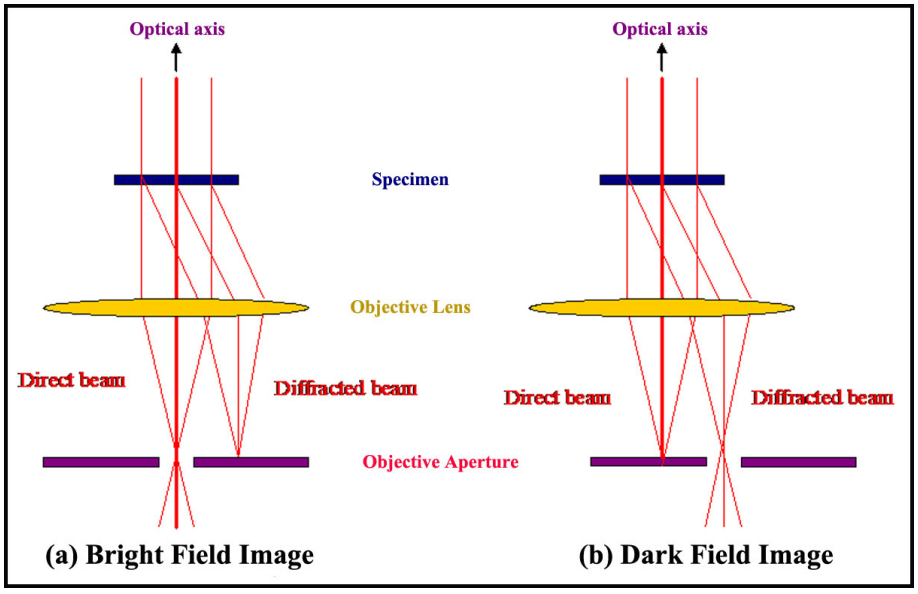

FIGURE 2.8: Ray diagram of (a) bright field and (b) dark field image formation in the TEM [145].

shown in Figure 2.8 (b). Since the DF image is formed by one of the many diffracted beams, thus the overall intensity of DF image will be much lower than BF image and it needs longer exposure time to get photographic image. However, low intensity will result in high contrast thus DF image typically has higher contrast than BF image [145]. Furthermore, specific diffraction spots can be selected in the back focal plane of the objective lens in order to form a DF image only from the electrons scattered by a chosen set of crystal planes. Such an image leads one to infer regions that contributed to the formation of such a diffracted spot.

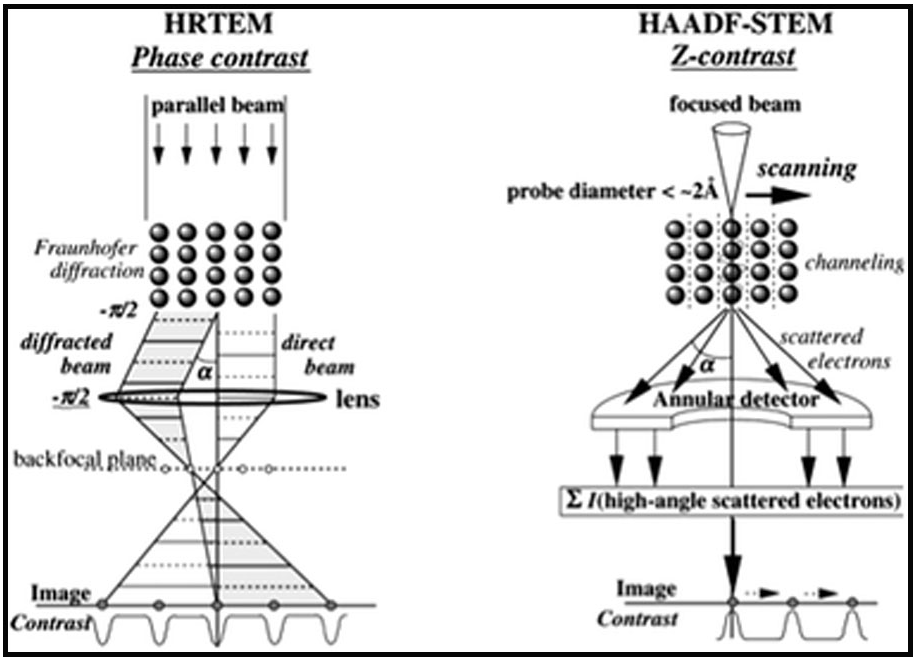

FIGURE 2.9: Schematics showing phase contrast and analytical imaging modes in TEM [149].

2.2.5 High resolution TEM (HRTEM)

One of the main strengths of the TEM is its point-to-point atomic resolution ability and is typically used to image metals, ceramics, mineral, nanostructured materials and

biological-related materials. They may provide information at atomic scale. The basic principle of HRTEM refers to tilting the electron transparent area of crystal to make the low-index direction exactly parallel to the incident electron beam. All the lattice planes which are almost parallel to the incident electron beam will be close enough to satisfy the Bragg law and diffract the primary incident electron beam. The formed diffraction pattern is actually the Fourier transform of the periodic potential for the electrons in two dimensions [134, 150]. When electrons passing through objective lens, the direct beam and all the other diffracted beams will be combined together again, the interference among all the beams will provide an inverse transformation and result in the formation of enlarged image of the periodic potential at the back focal plane of the objective lens. This image will be further magnified by the intermediate and projection lens system and finally projected on the fluorescence screen. Figure 2.9 gives schematic illustration of high resolution phase contrast and HAADF modes of TEM respectively. The resolution of TEM can be calculated by following equation

$$s = \frac{0.91\lambda}{NA} \tag{2.1}$$

where s is the resolution, λ is the wavelength of high energy electrons (i.e. for 200 keV electrons, $\lambda \sim 0.025$Å), and NA is the numerical aperture (for electron microscopy, NA $\sim$0.01 due to electron lens imperfections) [150]. A representative HRTEM image of rice-starch stabilized Ag NPs with FFT as inset is shown in Figure 2.10.

2.2.6 High angle annular dark field - scanning transmission electron microscopy (HAADF-STEM)

STEM can access the Z-contrast. The "Z contrast" is due to the difference in atomic numbers that may be present in the specimen. High angle annular dark field (HAADF)-STEM is capable of imaging atomic clusters. This mode of imaging requires the intensity of the beam on a specific area of the specimen to be increased. In this case, the C2 is focused and the beam is most convergent. This reduces the image contrast and to form an image, the beam is scanned over the sample in this mode of operation. The beam is made

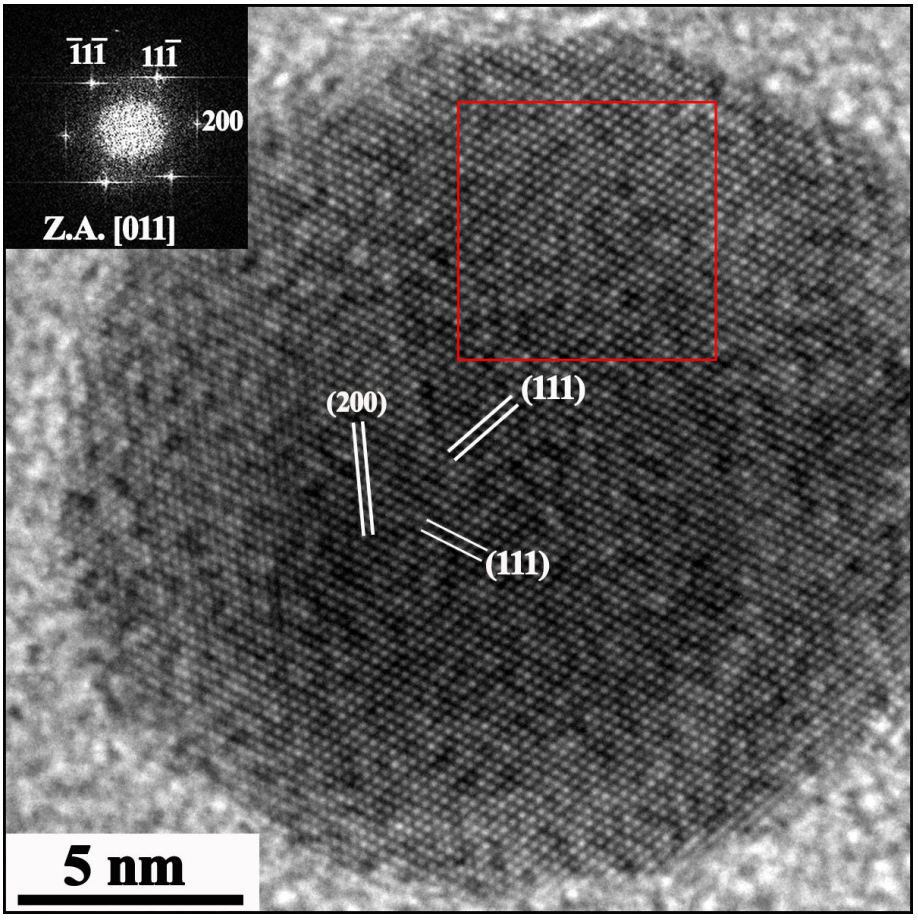

FIGURE 2.10: HRTEM image and FFT as inset obtained from rice-starch stabilized Ag NP colse to Z.A. [011].

parallel by using scan coils to pivot the beam about the front focal plane of the objective pole piece. The beam then emerges through a third condenser lens parallel to the optic axis to form the image on specimen plane. The quality of STEM images is dictated by the quality of the STEM detector. Figure 2.11 show a STEM image taken by the Tecnai G^2 T20 microscope and corresponding TEM BF image from Ag-Cu NPs. In STEM images, the brightest regions have high Z-value, i.e. element with high atomic number. In this case, the sample has both Ag and Cu NPs and the bright regions correspond to the Ag atoms in the sample.

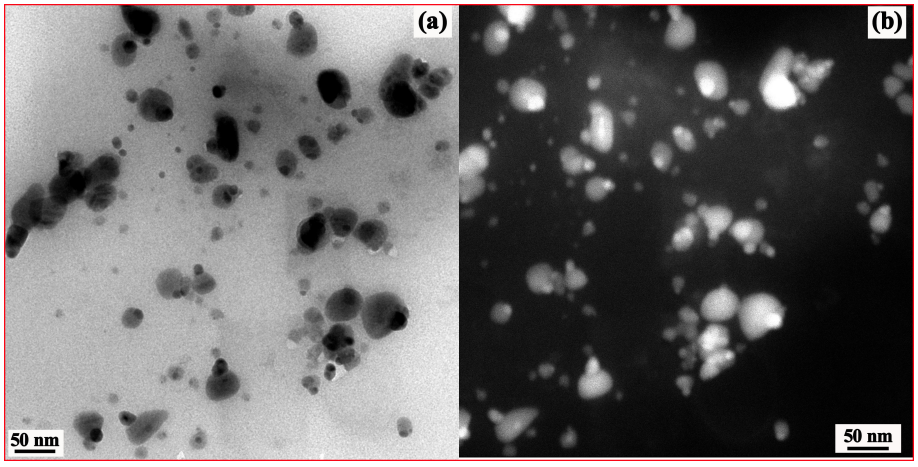

FIGURE 2.11: TEM BF image (a) and HAADF-STEM image (b) of Ag-Cu NPs

2.2.7 X-ray energy dispersive X-ray spectroscopy (EDS)

Electrons can eject a core electron from an atom in the sample because the energy of the electron beam is more than the binding energy of the core electrons. This causes X-ray-photons to be emitted with an energy equivalent to the energy difference caused by the movement of an electron from a higher orbital to the core shell. The X-ray photon emitted is characteristic of a particular element. The EDS analysis uses a detector placed above

the sample to count and analyze the energy of the X-rays emitted by the sample. The EDS data consists of an energy spectrum of the emitted X-rays in the range 0-20 keV in which elements can be identified from the spectral peaks. EDS analysis performed on bimetallic NPs can provide evidence of the relative compositions of their elements as shown in Figure 2.12 in the case of AuCu NPs.

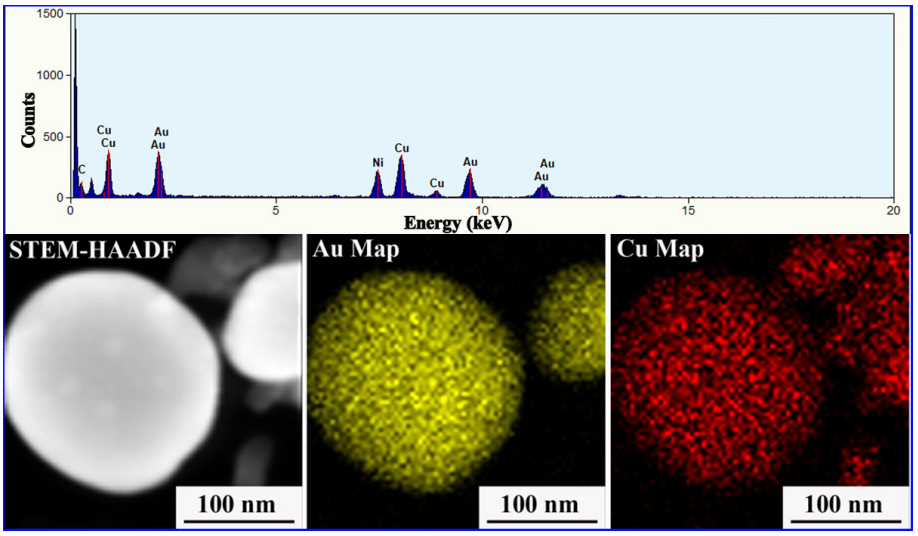

FIGURE 2.12: EDS spectrum and STEM-EDS elemental maps of Au-Cu alloy NPs.

2.2.8 Nano-beam diffraction (NBD)

It is very challenging to orient groups of small NPs along a zone axis and to capture the diffraction pattern, it is therefore advantageous to use the fast Fourier transforms (FFT) of the HRTEM images. Another alternative technique capable to capture DP from small NPs is convergence beam electron diffraction commonly known as micro-beam or nano-beam diffraction (NBD). In this, instead of parallel beam mode, TEM operates in convergence mode where beam can be converged down to $\sim$ 50 nm by changing strength of second

condenser lens (spot size) as well as inserting the smallest condenser aperture. The limitation of SAD aperture in acquiring DPs from NPs can be accommodated by making probe size $\sim$ 50 nm in NBD technique. NBD technique has been employed in this thesis (cf. chapters 4 and 7) to decipher structures at nanoscale. Figure 2.13 shows the SAD and NBD patterns recorded from Au and Cu NPs, respectively.

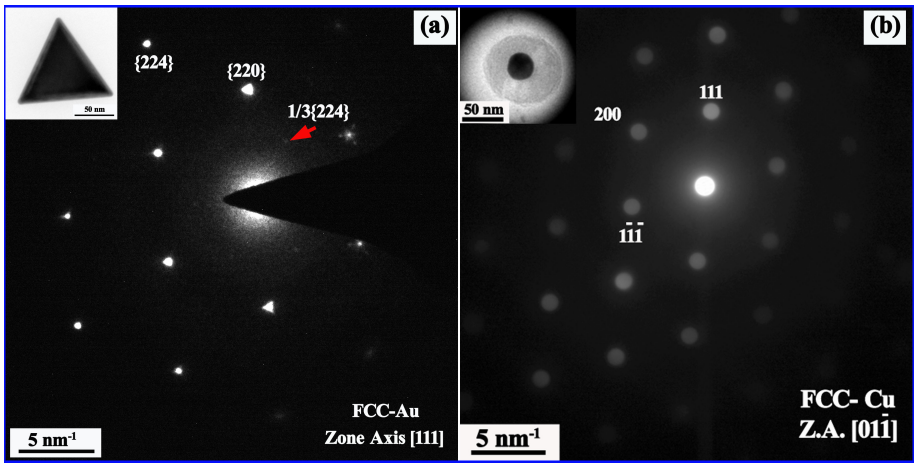

FIGURE 2.13: SAD and NBD patterns recorded from a single NPs of Au (a) and Cu (b), respectively.

In this thesis, HRTEM (FEI Tecnai G^2 T20 TEM) has been used to characterize the facet planes, twin boundaries etc. of the grown nanostructures. The point-to-point spatial resolution is 2.4 Å with an accelerating voltage of 200 kV. Figure 2.14 is the photograph of a Tecnai G^2 T20 TEM system which has been utilized in this work extensively. This system is attached with high angle annular dark field (HAADF) and X-ray energy dispersive spectroscopy (EDS) detectors. The TEM in scanning mode coupled with these detectors has been used to investigate the chemistry of the nanostructures. In addition to that, nano beam diffraction (NBD) patterns have been recorded to decipher localized structures by converging the beam down to $\sim$ 50 nm.

2.3 X-ray Diffraction (XRD)

Diffraction will occur when waves interact with a regular structure whose repeat distance is on the order of the wavelength and these common phenomena will satisfy by Bragg's law:

$$n\lambda = 2d\sin\theta \tag{2.2}$$

where λ is the wavelength of incident wave, d is the inter-parallel planes spacing (d-spacing) and θ is the diffraction angle in degrees. X-rays have wavelengths of the order of

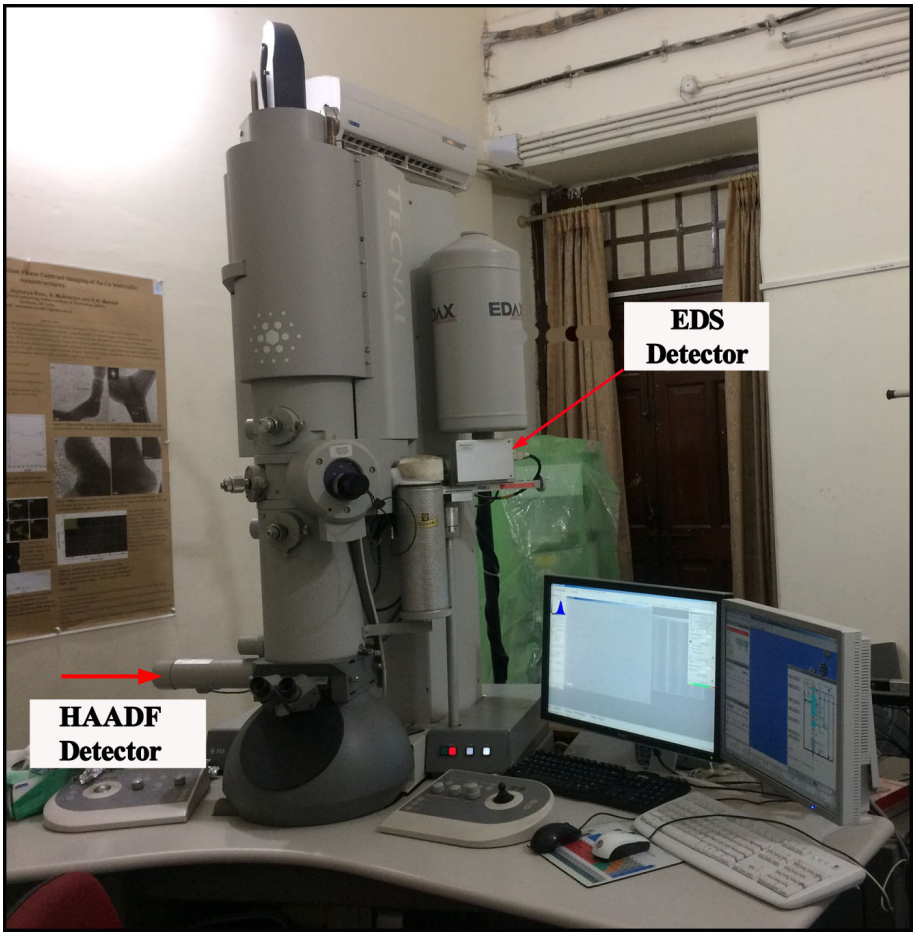

FIGURE 2.14: Tecnai G^2 T20 TEM system in Department of Metallurgical Engineering, IIT(BHU).

a few Å which are quite similar to the typical d-spacing in crystalline solids. Hence, X-ray can be scattered from a crystalline solid and produce a diffraction effects. Powder X-ray diffraction (XRD) is an analytical technique used to characterize the crystal structure and crystallite size (grain size), in polycrystalline materials.

In this thesis nanopowders has been investigated where XRD peak broadening is observed. The full width half maximum (FWHM) can be calculated from the peak in the diffraction pattern. This FWHM (denoted by β) can be used with Scherrer's formula to estimate average crystallite size. Scherrer's formula is given by

$$t = \frac{0.9\lambda}{\beta \cos\theta} \tag{2.3}$$

where t is crystallite size and θ is the Bragg angle [151]. β has been taken after making suitable corrections for instrumental broadening. Samples for XRD were obtained by centrifuging the sols. The X-ray diffraction of the powder was recorded by Rigaku X-ray diffractometer with Cu-Kα radiation with 40 kV excitation voltage and tube current of 30 mA. International Centre for Diffraction Data (ICDD) PDF4+ database was used to analyze the presence of various phases in diffraction patterns.

2.4 Study of stability of the sols

The localized surface plasmon resonance (LSPR) behaviour of the sols has been studied in this doctoral work using UV-Vis spectrophotometer. Nanoparticles dispersed in aqueous and organic media, absorption of incident radiation takes place due to localized surface

plasmon resonance (LSPR) of metal nanoparticles. The LSPR absorption wavelength is observed at specific wavelength depending on the nature of solvents as well as size and shape distribution of the dispersed nanoparticles. The instruments used for such studies was a Perkin-Elmer Lambda XLX+ and Agilent Cary 60 UV-Visible spectrophotometer. The measurements were carried out with an accuracy of 1 nm and a scan rate of 200 nm per minute. The measured range spanned from 200-800 nm and 200 - 1100 nm, respectively, for aforesaid UV-Vis spetrophotometers. The LSPR behavior of the sols and their stabilities were studied by recording UV-Vis absorbance spectra with respect to time.

Dynamic light scattering (DLS) is another equipment related to characterization of sol and estimate the stabilities by measuring zeta potential. The instrument used to study size distribution and zeta potential was Zetasizer, Malvern Instruments zeta-sizer Nano-ZS instrument.